Draft to appear in final form in the proceedings of the 2017 World Haptics Conference, pp. 575-580

Linear Induction Actuators for a Haptic interface: a quasi-perfect transparent mechanism

Alberto Ortega*, Antoine Weill-Duflos*, Sinan Haliyo*, Stéphane Régnier* and Vincent Hayward*

***Abstract*— This article describes the design of a high-fidelity haptic interface based on a two-axis induction system. Unlike other type of actuators, linear induction motors can provide simultaneously a non-contact drive and a very low inertia. Their integration in a haptic device enables an interface with quasi-perfect mechanical transparency. We detail the conception of linear induction motors for this application and experimental results of a proof of concept are shown.**

***Index Terms*— haptic device · haptic transparency · linear induction motor · low inertia**

I. Introduction

There exists no current haptic device that achieves perfect structural transparency. Their mechanical structure comes with large handle inertia and/or limited dynamic range, resulting in a low level of transparency blurring and masking the perception of small or highly dynamic phenomena that are so important to the human somatosensory system. Some of them achieve high degree of transparency with dedicated control scheme, but the usual conservative approach results in an ensured stability and a limited transparency [1] [2]. In other works high mechanical transparency has been achieved in single-axis interfaces using a dual-stage actuator technique [3].

In this paper we propose a three degree of freedom haptic device with a natural quasi-perfect transparent mechanism. The central technical objective is to eliminate any type of articulated joint in the structure, as well as the sources of friction and inertia. The preliminary concept calls for guiding very light and rigid moving part by an air-bearing technique and to actuate it without contact through an innovative two-axis induction system based on linear induction actuators. In Section II the concept of transparency is presented and related to the choice of linear induction motors as actuators for a haptic interface. Section III gives the fundamentals of linear induction motors and in Section IV the design criteria of the haptic interface are detailed. Section V describes the proof of concept assembly and in Section VI some experimental measurements are carried out. Section VII presents concluding remarks and gives recommendations for the further development of the haptic device.

*are with Sorbonne Universités, UPMC Univ Paris 06, UMR 7222, ISIR, F-75005, Paris, France. {ortega, weill, haliyo, regnier, hayward}@isir.upmc.fr

II. Actuators for a transparent mechanism

The main objectif of a high fidelity interface is to provide a faithful transmission of signals to couple the operator as closely as possible to the remote environment. Ideally, the interface would be perfectly transparent and it would make the operator feel that he his interacting directly with the remote environment [1][4]. The idealized teleoperation system with perfect transparency is usually designated as a massless, infinitely rigid stick [5].

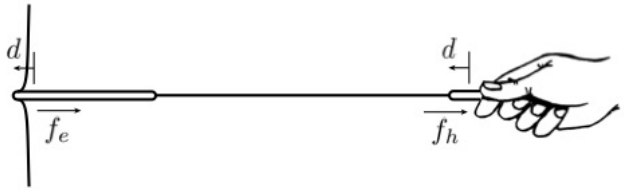

Fig. 1. Idealized teleoperator [6]

In a haptic interface, high transparency depends on reducing the parasitic forces under the smallest human detectable force under all desired operating conditions [7]. The magnitude of these parasitic forces ows mainly to friction and inertia. Removing every mechanical joint and reducing to the minimum the inertia of an interface would make it reach a structure with a high degree of mechanical transparency. Based on that, the use of electromagnetic machines and non contact forces in a haptic device would increase the fidelity of the manipulation.

Different kind of electromagnetic machines allow a non-contact transmission of forces. Since a two-axis system of actuation is desired, the analyze will be constrained to linear electromagnetic machines. These latter can be categorized into four categories: Linear Synchronous Motors (LSM), Linear Direct-current Motors (LDM), Linear Pulse Motors (LPM) and Linear Induction Motors (LIM). To allow unrestricted free exploration, the inertia of the device should be kept to a minimum [8]. The category with the lightest secondary or moving part and consequently the lowest inertia is the linear induction motor, which can have different topologies. The best solution to avoid the steel in the secondary that would increase the inertia is the double-sided topology instead of the single-sided. Thus double-sided linear induction motors (DLIM) were considered as very well suited actuators to achieve high mechanical transparent devices.

III. Linear induction motors' theory

Based on the theory of linear induction motors [9], some important parameters have to be considered during their design. One of them is the goodness factor G. This metric, developed by Eric Laithwaite, is related to the motor performance and it enables the efficient development of a LIM [10].

$$G = \frac{2 \cdot \mu_0 \cdot f \cdot \tau^2}{\pi \cdot \rho_s \cdot g} \tag{1}$$

where $\mu_0 = 4\pi \cdot 10^{-7} H \cdot m^{-1}$ is the permeability of the air, f is the source frequency in Hz, τ is the pole pitch of the primary winding in m, ρ_s is the surface resistivity of the secondary conducting sheet in $\Omega \cdot m^{-2}$, g is the airgap in m. This is an idealized metric that do not take into account certain phenomena inherent to the linear induction motors' nature, such as the airgap leakage, the secondary-sheet skin effect, and transverse edge effects [11].

Another important parameter for the DLIM design is its thrust F_x. This latter is given by the following equation:

$$F_x = \frac{3 \cdot \pi \cdot L_m \cdot {I_1}^2 \cdot s \cdot G_e}{\tau \cdot (1 + s^2 \cdot G_e^2)} \tag{2}$$

where I_1 is the rms value of primary phase current in A, s is the slip, $G_e = G/k_1$ where k_1 is a coefficient that takes into account edge effect, Joule effect, skin effect, airgap fringing and stator slotting. L_m is the magnetization inductance in H and it is given by

$$L_m(w_1) = \frac{6 \cdot \mu_0 \cdot (2a_e) \cdot (k_{w1} \cdot W_1)^2 \cdot \tau}{\pi^2 \cdot p \cdot g_{e_{Al}} \cdot (1 + k_{ss})} \tag{3}$$

where w_1 is the primary angular frequency (in rad/s), k_{w1} is the winding factor, W_1 is the turns in series per phase, d_{Al} is the secondary sheet thickness in m, $a_e = a + \frac{g_e Al}{2}$ in m , p is the number of pair of pols, $2a$ is the stack width in m, $g_{e_{Al}} = (2 \cdot g + d_{Al}) \cdot k_2$ in m where k_2 is a coefficient that takes into account the slot opening and the airgap fringing, k_{ss} is a coefficient that takes into account the stator magnetic saturation. As seen in equation 2, small variations in I_1 induce great variations in the thrust.

IV. Design of linear induction motors for a haptic interface

A. Performance criteria

Inspired by commercial touch-pads but aiming for smaller sizes in this first prototype, the workspace was define as a 50x50 mm square. Target values specifying the characteristics of a haptic interface that can operate at the limits of human performance have already been suggested [3]. Based on that, the moving part of the interface was limited to 50 g. Considering the smooth manipulation of the interface, where the user would drive the moving part with one up to three fingers, the maximum force was 2 N. It is worth to indicate that no time-domain performances were taken into account since the LIM's dynamic was estimated to cover all the human motor capabilities.

B. Design approach

As a first approximation most of the side effects were ignored and the coefficients were define as: $k_{w1} = k_1 = 1$ and $k_{ss} = 0$. Considering the wished relative compactness of the prototype and the workspace target value, some geometrical values were set arbitrarily: $2a = 30mm, g = 2mm, d_{Al} = 0.5mm$ and length of the motor $l = 125mm$.

Regarding the haptic performance of the interface, a thrust of 2 N per motor was considered enough. An oversizing design strategy was adopted with $F_x = 6N$ the maximum thrust and $I_1 = 2A$ the current to reach this thrust. Being $l = 125mm$ the motors' length and 3 the number of phases, 12 was contemplated as an appropriate number of slots in each motor. With such a number of slots and the two-layer three-phase winding of Fig 2, the number of poles resulted $2p = 4$.

$$\tau = \frac{l}{2p}$$

which gives $\tau \approx 31mm$. With all these numbers in equation 3:

$$L_m(w_1) \approx 8.79 \cdot 10^{-8} \cdot W_1^2$$

The optimum goodness criterion [11] suggested $Ge = 10$ for $2p = 4$. Expecting a low slip $s = 0.1$, equation 2 gave:

$$6 \approx 5.52 \cdot 10^{-5} \cdot W_1^2$$

and finally $W_1 \approx 358$.

Since there are 3 coils in series per phase, the number of turns per coil is given by

$$N_{coil} = \frac{W_1}{3}$$

After all these approximative design, it arised $N_{coil} = 120$ turns/coil.

C. Primary: electrical steel core with built-in winding

The raw material used for each linear induction motor are prisms of 30x30x120mm made of insulated sheets of M530-50A steel. This latter corresponds to electrical steel non grain oriented and presents a high relative permeability. To mechanize the slots and keep the laminated steel assembled, a machining process with low efforts was required. The solution adopted was the wire electrical discharge machining (WEDM).

Once the core of the linear induction motor was mechanized, the coils were built-in. With 9 individual coils, 3 per phase, the assembly was disposed following Fig 2. Finally the core with built-in coils was covered with resin, having just access to both extremities of each phase.

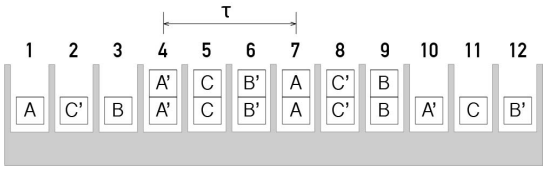

Fig. 2. Double-layer winding disposition.

D. Secondary: the moving part

The secondary has to be a paramagnetic and electrical conductive material, and the higher the electrical conductivity is, the higher the thrust induced on the secondary is [12]. Being a low inertia of the moving part of the haptic interface one of the main technical objectives, materials with a low density were prioritized. In this case the material with the best weight/conductivity ratio was the aluminum. Regarding geometrical parameters, the secondary had to be thin enough to permit a small airgap in the DLIM as well as a low amount of parasite currents. Its width should permit a good dissipation of the warmth and a good thrust, being the pole pitch of the primary winding τ a lower limit for it. Experimentally we realized that a wider secondary would reduce the vibrations felt while manipulating the interface. With all this considerations the secondary of the DLIM resulted in a 0.5-mm-thick and 5-mm-wide sheet of 1050 aluminum alloy.

V. Contact Free-Haptic Interface

As already mentioned, one of the central objective with this haptic interface is to eliminate any type of articulated joint in the structure. This is reached with a two-axis motor system based on linear induction motors, whose layout is shown in the Fig 3. Considering that each DLIM induces a unique longitudinal force, at least 3 of them are required to cover a two-dimension working space. With this system, X and Y forces as well as a torque in the Z-direction can be induced over a moving aluminium plate. This interface claims to eliminate the sources of inertia and friction and the different parts of the interface are conceived to reduce them as much as possible.

A. Moving plate and air-bearing

In a haptic interface, friction and inertia are the main sources of parasitic forces that distort the perception of physical phenomena. The induction system based on three DLIMs eliminates all the friction related to the drive, but there is still the friction related to the displacement of the moving part. To reduce it, an air-bearing technique was adopted. The idea is to manipulate the moving plate of the interface over a thin film of pressurized air, the same way the puck on an air hockey table is ”floating” on air. Gas film bearings allow a clean working conditions and they operate with zero static and dynamic friction where liquid fluid film bearings have much higher friction and pumping losses. To

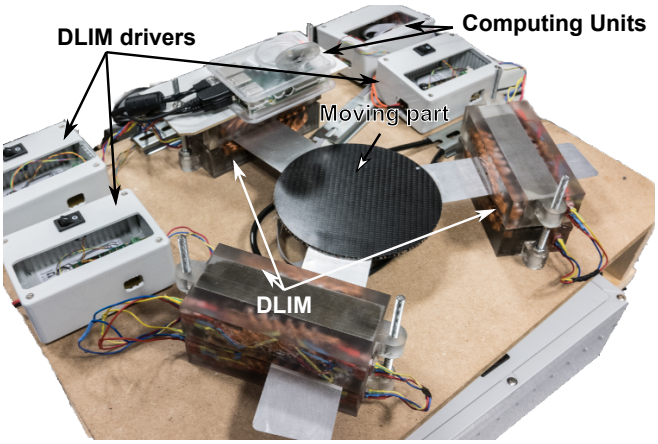

Fig. 3. Haptic interface with an actuation based on linear induction motors.

maintain a constant air gap and maximize the stiffness of the air bearing, a preload is required. The preferred solution was vacuum preload, since it helps to maintain constant air gap without adding unnecessary moving mass, which is essential for the low inertia objective of the moving plate. Thus, a small commercial vacuum preloaded air bearing (model S205001; New Way Air Bearings) was integrated in the interface.

Another central objective was to achieve a very low handle inertia, a property that has been demonstrated to be fundamentally important for optimal coupling with the operator [13], [7]. Considering the actuators characteristics, a 0.5-mm-thick and 5-mm-wide sheet of 1050 aluminum alloy was chosen as secondary for the DLIMs. Nevertheless, the vacuum preload induces bending stresses that would deform the aluminum. A structure offering excellent rigidity and minimal weight is the carbone fiber with aramid honeycomb core. This composite material was then used as the ”puck” floating on the air bearing, and on it three 0.5-mm-thick and 5-mm-wide sheets of 1050 aluminum alloy would be stuck, each one corresponding to the secondary of each linear induction motor.

B. Impedance control

Bi-directional information flow is the most distinguishing feature of haptic interfaces. To control them, there are two main types of strategies: the impedance-control and the admittance-control. The impedance-control is the most common and it is the one adopted for the prototype here presented. With this approach, the virtual environment defined specifies the forces that have to be generated by the device’s actuators in response to moving the device: a force is send and a displacement is measured [6]. Compared to the admittance-control it has a cheaper and easier implementation. A force control is also more interesting for the rendering of virtual textures, but it requires a device that reacts with large changes in forces to small changes in the position [14]. Thus, a precise measurement of the displacement is required, as well as a characterization of the

electrical impedance of the system to design the appropriate electronic.

1) Position sensing: The impedance-control requires the position sensing of the moving part. To preserve the mechanical transparency of the interface, a non contact method was preferred. Taking into account other parameters such as resolution, sensing speed and the kind of displacements to measure, the laser sensing was adopted. To measure the X and Y displacements as well as the Z-rotations over all the working space of the device, three laser motion sensor (model ADNS-9800; Avago) were arranged in the interface. To read the signals of the three sensors, a usb/based microcontroller (teensy 3.2; PJRC) was used. Each sensor has a frame rate up to 12,000 fps and even if the reading of the data of the three laser sensors was slower, update rates over the 1kHz required by the sense of touch were achieved.[15].

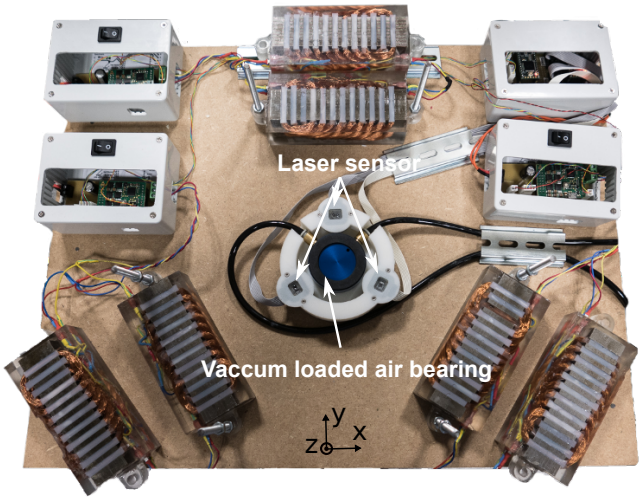

Fig. 4. Air bearing and position sensor system.

2) Electrical impedance of the linear induction motor: To create a moving magnetic field with the three-phase winding disposition of the laminated steel core, it was necessary to supply a three-phase signal. The most appropriate was a three-phase balanced sinusoidal signal. To find the electronic capable of doing that, the impedance value of the coils had to be calculated . Thee theoretical equations of a coil resistance R_{coil} and impedance L_{coil} are:

$$R_{coil} = \rho_{Cu} \frac{l_{Cu}}{S} \tag{4}$$

where $\rho_{Cu} = 1,68 \cdot 10^{-8} \Omega \cdot m$ is the resistivity of the copper, l_{Cu} is the length of the copper wire in m and S is the cross-sectional area of the copper wire in m^2

$$L_{coil} = \frac{\mu_0 \mu_r N_{coil}^2 S}{l_{Cu}} \tag{5}$$

where μ_r is the relative magnetic permeability of the material of the linear induction motor. This value varies with the magnetic field and at 0,002 Tesla for electrical steel $\mu_{r_{ElSteel}} = 4000$. This value will be taken for a first calculation.

The design of the single-sided motor was done considering a maximum current of 2A per phase, which following the tables of AWG wire sizes requires a wire with a diameter of $0,4mm$. With such a wire and with the geometry of the prototype, for a coil: $l_{Cu} \approx= 14400mm$ and $S \approx 0.823mm^2$, which with equations 4 and 5 gave: $R_{coil} \approx 2.9\Omega$ and $L_{coil} \approx 4.1 \cdot 10^{-5} H$.

The theoretical impedance of a coil is

$${Z_{phase}}^2 = R_{phase}^2 + (wL_{phase})^2 \tag{6}$$

where Z_{phase} is the impedance of one phase, R_{phase} is the resistance of one phase, w is the angular frequency of the phase's signal and,L_{phase} is the inductance of one phase.

With the equation 6 the impedance of a phase of the linear induction motor can be deduced. There are three coils per phase, and depending wether they are connected in series or in parallel, it results:
$L_{coil_{series}} \approx (8.7^2 + w^2 1.2 \cdot 10^{-4})^{\frac{1}{2}}$ and $L_{coil_{parallel}} \approx (0,97^2 + w^2 5.6 \cdot 10^{-10})^{\frac{1}{2}}$

As it will be explained later, the operational frequency of the induction motors had to be over 600Hz for a good haptic sensation. A series connexion of the coils and an operational frequency over 600 Hz would demand too high voltages. That is why the coils were finally connected in parallel.

3) DLIMs drivers: To drive the linear induction motors, three commercial 4-quadrant PWM servo controller for brushless EC motors were used(model ESCON Module 50/5; Maxon Motor). This controller can deliver 5A per phase at 50V, but to work they need the hall sensor signal that standard EC motors usually provide. In this case, the signal sets the working frequency of the linear induction motor and to recreate it artificially a teensy microcontroller was employed.

A single-board computer (model Raspberry PI 3) was used as central master: it collects the data from the teensy that reads the laser sensors, and with this information it sets the hall sensors signals of each motor. For that, the raspberry Pi 3 runs a program that takes into account the disposition of the linear induction motors and the virtual environment.

VI. Experimental measurements

The interface presented a moving plate of 55g and the feeling of inertia was very low while manipulating it over

the airbearing. For this latter the air compressor supply of the laboratory was used.

Working at 50Hz translated into a very uncomfortable manipulation of the interface. Indeed, the aluminum plates had a resonance at 300 Hz and provoked a "dead-finger" feeling. To remove it the solution was to work at higher frequencies, which increased the electrical impedance of the coils. To keep reasonable operational voltages, each phase coils connection was modified from a series connection of the original design to a parallel connection. Experimentally the working frequency was set to 660 Hz, which made the aluminum plates resonate at 4000 Hz and provided a more comfortable manipulation.

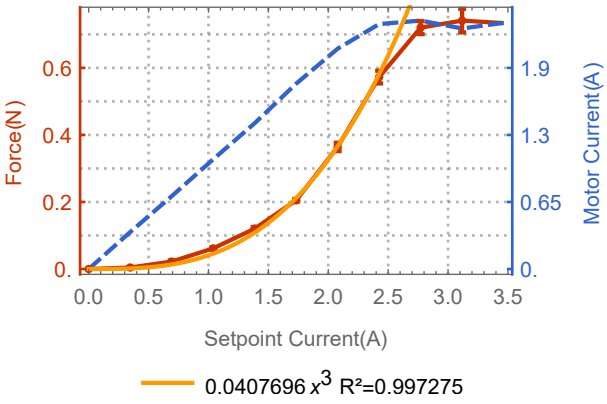

Fig. 5. Relation between the thrust of a linear induction motor (Force), the setpoint of current and the real output current of the electronic driver (Motor current)

For the measurements a force sensor was mounted on one of the aluminium plates and a digital scope recorded simultaneously the closed loop current of the electronic drivers and the force sensor signal. A thrust-intensity empirical relation is shown in Fig 5. Each point corresponds to the mean of ten measurements and their standard deviation is included in Fig 5. Around 2.2 A the electronic driver starts to limit its output current and then reaches a maximum value. The thrust increases despite the driver's saturation: this may be explained by the capacity of the amplifier to overcome this limit for a short amount of time. Below 2.2 A, the thrust-current quadratic relation expected from (2) appears empirically as a cubical function. This can be due to the electronic drivers solution adopted for this proof of concept.

The time constant of the interface was also measured empirically in Fig 6. Three different values are displayed: the force measured by the force sensor, the closed-loop current of the electronic drivers and the step signal (setpoint) sent to the device. An average of eighteen measurements is used and the standard deviation of the force is shown. The current presents a response time of 15 ms at 5% . Concerning the measured forces, the mean time constant is 25 ms ranging

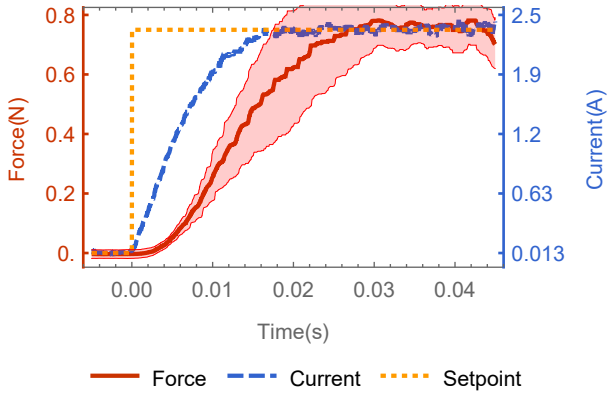

Fig. 6. DLIM response to a step

from 17 ms to approximately 30 ms. All the measurement where made on a single motor. Considering the disposition of the motors, this results can be applied to the interface. As shown in Fig 3, the motors are tangential to a circle of radius r and at 60 degrees one from each other. Based on the reference of Fig 4, the relation linking the interface forces and the ones delivered by the DLIMs are, :

$$F_{totx} = -F_1 + \frac{F_2}{2} + \frac{F_3}{2} \tag{7}$$

$$F_{toty} = -\frac{\sqrt{3}F_2}{2} + \frac{\sqrt{3}F_3}{2} \tag{8}$$

$$M_{tot} = r\sum_{i=1}^{3} F_i + x\frac{\sqrt{3}}{2}(F_2 - F_3) + y\left(\frac{F_2 + F_3}{2} - F_1\right) \tag{9}$$

with F_i the forces of the 3 DLIMs (the force is positive if it creates a positive torque), (x, y) the position of the moving plate, F_{tot} the total force of the device and M_{tot} the torque on the center.

VII. Conclusion and Discussion

We describe a haptic interface that works with a quasi-perfect structural transparency. Indeed, the drive system based on linear induction motors and the airbearing system eliminate any parasitic forces due to friction, leaving the very low inertia of the moving part as the last barrier to a perfect structural transparency. Experimental tests have shown an extremely smooth and comfortable haptic feeling of manipulation, but more control has to be implemented to reproduce virtual environments with high fidelity.

Not only control improvements but also design ones have to be pointed. Mutual inductances, non symmetrical disposition of the coils and Joule and end effects among others contribute to a non uniform thrust over the aluminum plate all along the DLIM. Different parameters could be tuned to achieve higher performances, such as the winding configuration to limit the end-effect or the number of

phases to reduce the feeling of creeks while working at low frequencies.

Linear induction motors are usually present in transportation and the theory related to them has been developed based on that. Their characteristics make them very well suited for haptic applications and further work should involve analytical study of this topic. Perceptual vibrations, compactness and thrust could be the basis of this new generation of haptic actuators.

ACKNOWLEDGMENTS

Special thanks to Bernard Javot for his manufacturing assistance and to Thomas Daunizeau for his engineering advice.

REFERENCES

[1] D. A. Lawrence, "Stability and transparency in bilateral teleoperation," *IEEE transactions on robotics and automation*, vol. 9, no. 5, pp. 624–637, 1993.

[2] A. M. Ousaid, A. Bolopion, S. Haliyo, S. Régnier, and V. Hayward, "Stability and transparency analysis of a teleoperation chain for microscale interaction," in *2014 IEEE International Conference on Robotics and Automation (ICRA)*, pp. 5946–5951, IEEE, 2014.

[3] G. Millet, S. Haliyo, S. Régnier, and V. Hayward, "The ultimate haptic device: First step," in *EuroHaptics conference, 2009 and Symposium on Haptic Interfaces for Virtual Environment and Teleoperator Systems. World Haptics 2009. Third Joint*, pp. 273–278, IEEE, 2009.

[4] S. Hirche, A. Bauer, and M. Buss, "Transparency of haptic telepresence systems with constant time delay," in *Proceedings of 2005 IEEE Conference on Control Applications, 2005. CCA 2005.*, pp. 328–333, IEEE, 2005.

[5] D. A. Lawrence and J. D. Chapel, "Performance trade-offs for hand controller design," in *Robotics and Automation, 1994. Proceedings., 1994 IEEE International Conference on*, pp. 3211–3216, IEEE, 1994.

[6] V. Hayward and K. E. MacLean, "Do it yourself haptics: part i," *IEEE Robotics & Automation Magazine*, vol. 14, no. 4, pp. 88–104, 2007.

[7] A. Mohand-Ousaid, G. Millet, S. Régnier, S. Haliyo, and V. Hayward, "Haptic interface transparency achieved through viscous coupling," *The International Journal of Robotics Research*, vol. 31, pp. 319–329, Mar. 2012.

[8] V. Hayward and O. R. Astley, "Performance measures for haptic interfaces," in *Robotics research*, pp. 195–206, Springer, 1996.

[9] I. Boldea, *Linear electric machines, drives, and MAGLEVs handbook*. CRC Press, 2013.

[10] E. Laithwaite, "The goodness of a machine," *Electrical Engineers, Proceedings of the Institution of*, vol. 112, no. 3, pp. 538–541, 1965.

[11] I. Boldea and S. Nasar, "Optimum goodness criterion for linear-induction-motor design," *Electrical Engineers, Proceedings of the Institution of*, vol. 123, no. 1, pp. 89–92, 1976.

[12] H. Noma, S. Yoshida, Y. Yanagida, and N. Tetsutani, "The proactive desk: A new haptic display system for a digital desk using a 2-dof linear induction motor," *Presence: Teleoperators and Virtual Environments*, vol. 13, no. 2, pp. 146–163, 2004.

[13] A. Mohand Ousaid, G. Millet, S. Haliyo, S. Régnier, and V. Hayward, "Feeling What An Insect Feels," *PloS ONE*, vol. 9, no. 10, p. e108895, 2014.

[14] M. A. Otaduy and M. C. Lin, "High fidelity haptic rendering," *Synthesis Lectures on Computer Graphics and Animation*, vol. 1, no. 1, pp. 1–112, 2006.

[15] V. Hayward, O. R. Astley, M. Cruz-Hernandez, D. Grant, and G. Robles-De-La-Torre, "Haptic interfaces and devices," *Sensor Review*, vol. 24, no. 1, pp. 16–29, 2004.